Available online at www.sciencedirect.com

ScienceDirect

journal homepage: http://www.elsevier.com/locate/acme

Original Research Article

Effects of superimposed hydrostatic pressure on bulging deformation and fracture of tubes in double-sided hydroforming

Xiao-Lei Cui [a,b,*], *Shi-Jian Yuan* [b]

[a] *College of Materials Science and Engineering, Taiyuan University of Technology, Taiyuan 030024, China*
[b] *National Key Laboratory for Precision Hot Processing of Metals, Harbin Institute of Technology, Harbin 150001, China*

ARTICLE INFO

Article history:
Received 12 June 2018
Accepted 30 December 2018
Available online 25 January 2019

Keywords:
Hydrostatic pressure
Hydroforming
Fracture
Bulging deformation
External pressure

ABSTRACT

Finite element analysis and scanning electron microscope were conducted to investigate the bulging deformation and fracture of tubes in double-sided hydroforming. The effect of the external pressure imposed on the tube, which determines the magnitude of superimposed hydrostatic pressure, on the stress state, yield locus, fracture surface formation, and fracture strain was evaluated. The simulation results revealed that sufficiently high external pressure can change the stress state of the tube in double-sided hydroforming from an in-plane biaxial tensile stress state to a three-dimensional stress state, and it can increase its hydrostatic pressure in a superimposed manner. Moreover, double-sided free bulging and corner filling experiments were conducted on 5A02 aluminum alloy and 2A12 aluminum alloy tubes. It was found that the external pressure has a significant impact on the fracture behavior of these tubes. The increasing external pressure could change the type, number, size, and proportion of the dimples on the fractured surface, and transform the fracture mode from a void accumulation fracture to a pure shear fracture, which significantly improves the fracture limit of the tubes. These results are significant for the consolidation of the theoretical and numerical simulation prediction of the superimposed hydrostatic pressure effect in the hydroforming process.

1. Introduction

In recent times, tube hydroforming technology attracted considerable attention in the automobile and aerospace industries, for its superior manufacturing capabilities with respect to lightweight integral hollow-structure components [1]. During the hydroforming process, the tubes are bulged under internal pressure and independent axial feeding. Due to the negligible through-thickness normal stress induced by the internal pressure, when compared with the in-plane stresses, the stress state on the tube is always simplified as a plane

* *Corresponding author at*: College of Materials Science and Engineering, Taiyuan University of Technology, Taiyuan 030024, China.
E-mail addresses: cuixiaolei2005@163.com, cuixiaolei@tyut.edu.cn (X.-L. Cui).

https://doi.org/10.1016/j.acme.2018.12.012
1644-9665/

stress state; i.e., axial compressive stress and circumferential tensile stress in the first forming stage, and biaxial tensile stress in the subsequent calibration stage [2]. Under such a stress state, several failures such as localized wrinkling and cracking [3] are easy to occur on the tubes, especially with the aluminum alloy [4] and magnesium alloy [5] tubes with an intrinsic low ductility [6]. Consequently, several studies have been conducted on the tube bulging deformation and fracture in the hydroforming process [7].

It is probable that premature ruptures occur before the complete formation of the aluminum alloy and magnesium alloy tubes; thus, a method to improve their ductility is required, for example, changing the stress state in the forming process [8]. In practice, following the studies by Bridgman [9], a significant number of studies on the effect of hydrostatic pressure on the formability of a variety of engineering materials were conducted [10]. These materials are mainly polycarbonate [11], brass [12], copper [13], steel [14], and aluminum alloy [15]. The ductility of these materials increases in accordance with an increase in the hydrostatic pressure. In addition, their fracture strains were also found to increase significantly with an increase in hydrostatic pressure. It should be noted that all of these studies were focused on either the round bar [16] or the sheet [17] tensioned uniaxially at the desired level of the superimposed hydrostatic pressure.

Based on the above results, researchers in the manufacturing field introduced the superimposed pressure effect into the metal forming process [18], such as the double-sided tube hydroforming process [19]. In double-sided tube hydroforming, the external pressure is exerted on the outer surface of the tube coupled with the internal pressure. In this case, the through-thickness normal compressive stress induced by the external pressure cannot be ignored, and the stress state changes from the plane stress state to the three-dimensional (3D) stress state. In particular, the hydrostatic pressure imposed on the tube increases simultaneously. Recently, researchers [20] established several theoretical models based on the classical plastic instability theory and M-K theory, to predict the effect of the through-thickness normal stress on the deformation ability of sheet and tube metals. The conclusions obtained was that the theoretical formability increases due to the through-thickness normal stress, and that the forming limit curves (FLCs) are shifted upwards along the major strain axis when the normal compressive stress increases [21]. However, almost no systematic experimental study was conducted until a dedicated experimental setup for the double-sided tube hydroforming process was established by our research group [22]. In the preceding work, our main focus was on the experimental verification of the effect of external pressure on the uniform deformation behavior of aluminum alloy tubes before the necking occurrence. It was found that the external pressure has little influence on the forming limit strain before necking [23].

With respect to the fracture behavior of tubes under double-sided hydroforming, a limited number of studies under the relative low external pressure [$1.5\sigma_s$ (127.5 MPa)] were discussed in the paper [24]. It was preliminarily found that a higher external pressure (superimposed hydrostatic pressure) applied on the outside surface of the tube can affect the fracture morphology of a 5A02 aluminum alloy tube in the double-sided hydroforming of a square section, and significantly improve its fracture strain. Recently, Shi et al. [25] used the numerical simulation to evaluate the effect of the superimposed hydrostatic pressure on necking (uniform stain and localized necking), fracture initiation, and fracture surface formation in double-sided tube hydroforming. In the study, an axisymmetric finite element model was established. However, the axisymmetric finite element model could only be used to evaluate the bulging deformation before necking and the fracture development in the circumferential direction. In addition, it was reported that the axisymmetric methodology cannot be used to differentiate the fracture development in the circumferential direction from the axial direction. In practice, the fracture always develops in the axial direction [24]. It is therefore necessary to further investigate the effect of superimposed hydrostatic pressure on the deformation and fracture of tubes in double-sided hydroforming, especially the experiment under higher external pressures or other hydroforming modes.

In this paper, a detailed numerical investigation of the bulging deformation behavior was firstly carried out, to conduct the stress analysis of the tubes under the effect of superimposed hydrostatic pressure in double-sided tube hydroforming. Furthermore, 5A02 aluminum alloy tubes and 2A12 aluminum alloy tubes were bulged freely and in a square-section die cavity under double-sided pressures in the experiments. The fracture behavior of the tubes under the effect of superimposed hydrostatic pressure are discussed in detail with respect to the experimental results.

2. Preparations

2.1. *As-received tube materials*

The as-received tube materials used in this investigation were 5A02 aluminum alloy tube and 2A12 aluminum alloy tube. The 5A02 aluminum alloy tubes were drawn from extruded tubes and then annealed at 380 °C for approximately 2 h, with outer diameter of 63 mm and nominal thickness of 2 mm. The 2A12 aluminum alloy tubes were annealed samples from hot-extrusion, with outer diameter of 66 mm and nominal

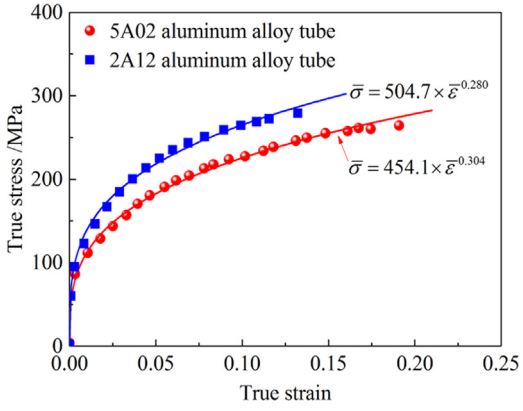

Fig. 1 – True stress–strain curve of as-received tube materials along the axial direction.

Table 1 – Mechanical properties of as-received tube materials along the axial direction.

Mechanical parameters	Values	
	5A02 tube [24]	2A12 tube
Initial yield stress, σ_s (MPa)	85.9	96.9
Ultimate tensile strength, σ_b (MPa)	222.9	246.5
Total elongation, δ_u (%)	26.1	23.5
Uniform elongation, δ (%)	18.2	15.3
Strength coefficient, K (MPa)	454.1	504.7
Strain hardening exponent, n	0.304	0.280

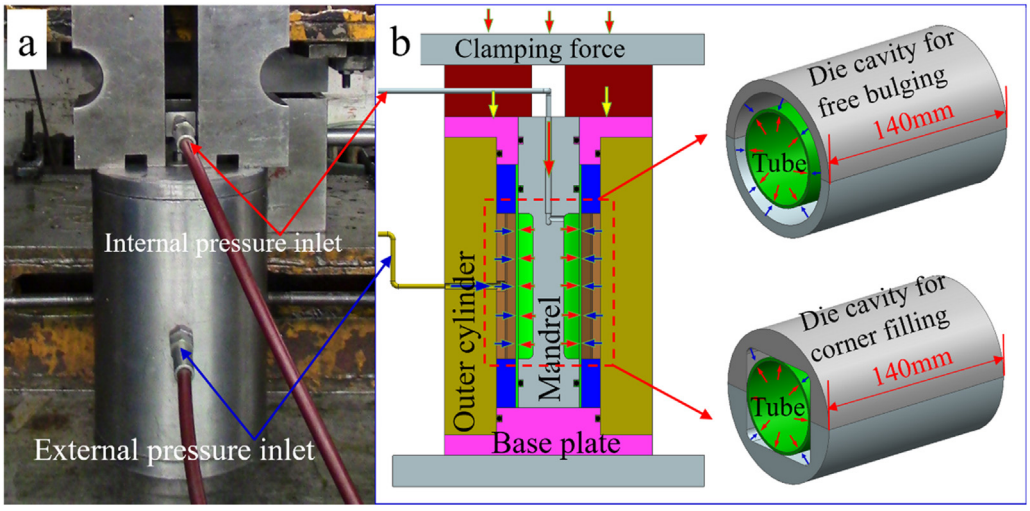

Fig. 2 – Double-sided tube hydroforming experimental setup [22]: (a) hydroforming die in operation; (b) schematic diagram of internal structure of the die.

Table 2 – Loading paths for double-sided hydroforming of 5A02 and 2A12 aluminum alloy tubes.

Materials	Loading paths	Pressure (MPa)							
		a (free bulging)				b (bulging in square-section die)			
		T_0	T_1	T_2	T_3	T_0	T_1	T_2	T_3
5A02	1 ($p_e = 0$) [24]								
	p_i	0	0	15	0	0	0	25	0
	p_e	0	0	0	0	0	0	0	0
	2 ($p_e = 1.0\sigma_s$) [24]								
	p_i	0	90.8	100	0	0	90.8	110	0
	p_e	0	85	85	0	0	85	85	0
	3 ($p_e = 1.5\sigma_s$) [24]								
	p_i	0	136.1	142.5	0	0	136.1	152.5	0
	p_e	0	127.5	127.5	0	0	127.5	127.5	0
	4 ($p_e = 2.5\sigma_s$)								
	p_i	0	217.5	227.5	0	0	217.5	237.5	0
	p_e	0	212.5	212.5	0	0	212.5	212.5	0
2A12	5 ($p_e = 0$)								
	p_i	0	0	25	0				
	p_e	0	0	0	0				
	6 ($p_e = 1.0\sigma_s$)								
	p_i	0	106.7	122	0				
	p_e	0	97	97	0				
	7 ($p_e = 2.0\sigma_s$)								
	p_i	0	213.4	219	0				
	p_e	0	194	194	0				

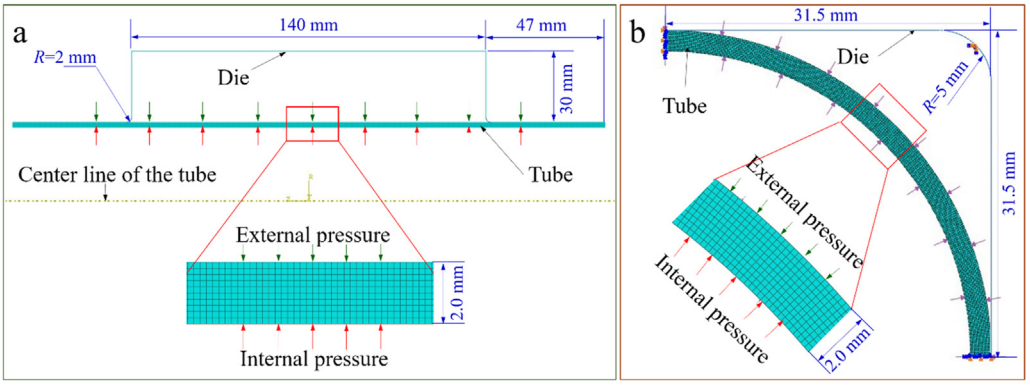

Fig. 3 – Numerical simulation model of tube deformation under internal and external pressures: (a) free bulging; (b) corner filling [22].

thickness of 3 mm. The uniaxial tensile tests were conducted on an Instron 5569 machine along the axial direction of the two types of tube materials. Their true stress–strain curves are presented in Fig. 1, and the corresponding mechanical parameters are listed in Table 1.

2.2. *Double-sided hydroforming experiment*

Fig. 2 shows the specially designed experimental setup for double-sided tube hydroforming, and a schematic diagram of the internal structure of the die was provided for clarity.

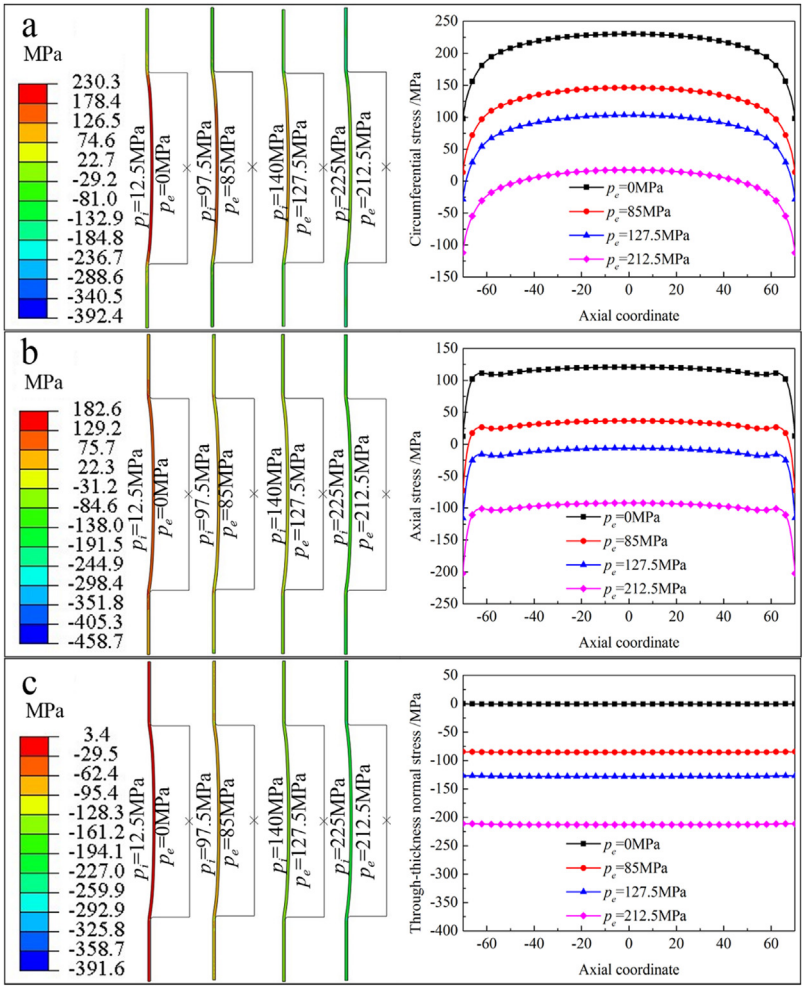

Fig. 4 – Stress distribution of 5A02 tubes in free bulging under internal and external pressures: (a) circumferential stress; (b) axial stress; (c) normal stress.

Considering a safety factor of $N_s = 1.2$, the sealed cylinder can withstand a maximum external pressure of 240 MPa. More detailed descriptions about this experimental setup can be found in the published literatures [22].

During the hydroforming process, the expansion of the tube is driven by the pressure difference between the increasing internal pressure and the constant external pressure. Different superimposed hydrostatic pressures can be introduced according to the change in the external pressure. The loading paths can be found in the literature [24], and the detailed load history data are presented in Table 2. In Table 2, the pressures at the T_2 moment are sufficiently high to crack the tubes. The fracture behavior of 5A02 aluminum alloy tubes under loading paths 1b, 2b, and 3b were discussed preliminarily in the double-sided hydroforming with square-section die. In this paper, to explorer the effect of higher superimposed hydrostatic pressures, path 4 (higher external pressure) was used in the investigation. Moreover, the fracture behavior of the 5A02 and 2A12 aluminum alloy tubes in the free bulging process was also investigated. In this case, loading paths 1a, 2a, 3a, and 4a were used for the 5A02 tubes, whereas loading paths 5a, 6a and, 7a were used for the 2A12 tubes. In the experiments, all the used tubes had a total length of 234 mm, and the length of bulging area was 140 mm.

2.3. *Fracture analysis*

To reveal the effect of superimposed hydrostatic pressure on the fracture behavior of tubes in double-sided hydroforming, a FEI Quanta 200FEG scanning electron microscope (SEM) was

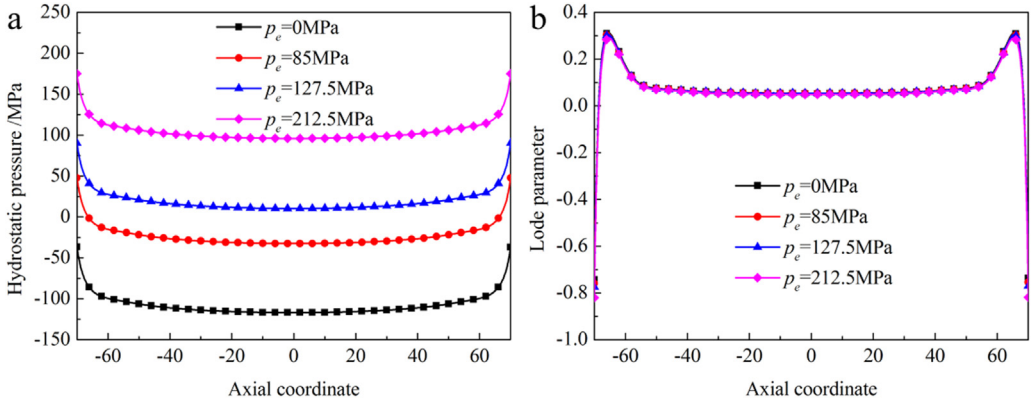

Fig. 5 – Hydraulic pressure and Lode parameter of 5A02 tubes under internal and external pressures: (a) hydraulic pressure; (b) Lode parameter.

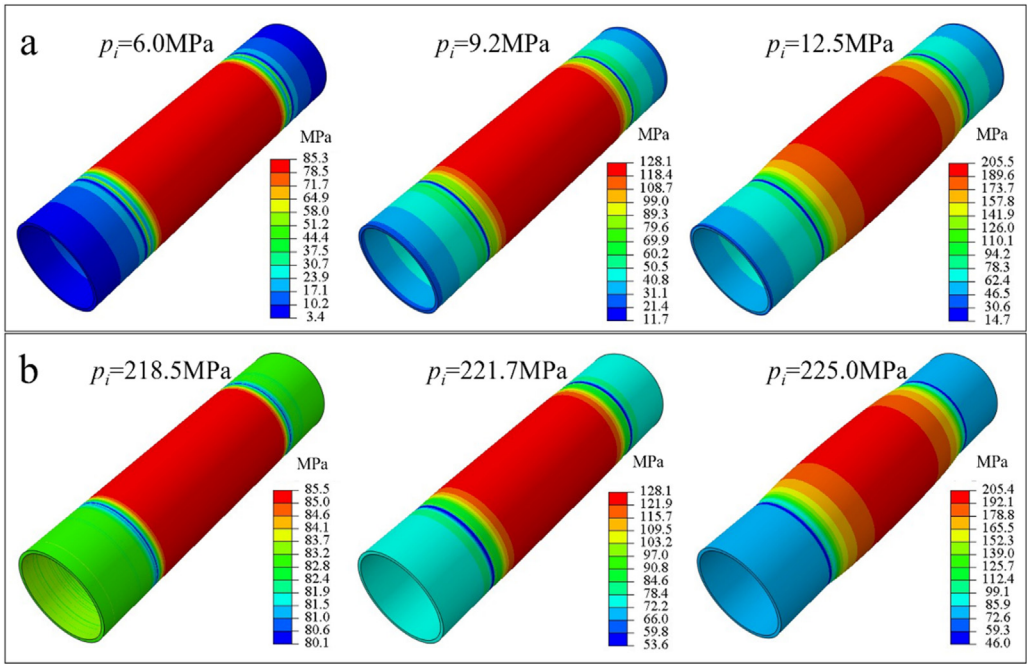

Fig. 6 – Equivalent stress distribution of 5A02 tube free bulging under internal and external pressures: (a) p_e = 0 MPa; (b) p_e = 212.5 MPa.

used for the fracture surface observation. First, the fracture morphologies under different external pressures were compared to distinguish the transformation of the fracture mode. Second, the thicknesses of the tubes at the fracture were measured on the SEM images with a 100× magnification, to calculate the fracture strain of the tubes.

2.4. *Finite element model*

The general finite element analysis software ABAQUS/Explicit was used to conduct the simulation of the double-sided tube hydroforming process of aluminum alloy tubes with a dynamic explicit analysis. Fig. 3 presents the established finite element model of the tube free bulging and corner filling deformation under double-sided pressures. In general, the shell element was used to model the deformable sheets or tubes in the forming process due to the negligible through-thickness normal stress. However, the solid element should be used to construct the tubes subjected to double-sided pressures, for the consideration of the superimposed hydrostatic pressure. For the tubes deformed under the three-dimensional (3D) stress state, a 3D model should be constructed. However, with the consideration of a significant number of elements for the 3D model, the simplified solid element model is recommended.

In the free hydro-bulging process, the tube and the die were established with an axisymmetric model according to their symmetrical features. The CAX4R elements (a four-node bilinear axisymmetric quadrilateral, reduced integration, hourglass) were assigned to the tube, and it was divided into ten layers along the thickness direction with an element size of 0.2 mm. For the corner filling process in a square die, a one quarter plane strain finite element model was established. The tube metal was modeled by the plane strain solid elements CPE4R (a four-node bilinear plane strain quadrilateral, reduced integration, hourglass control), and it was also divided into ten layers along the direction of the thickness. All the dies were defined as analytic rigid shells. In addition, the isotropic hardening model (annealed tubes) and the surface to surface contact relationship were adopted in these simulations. The loading paths used in the simulation were the same as that in the experiment, as shown in Table 2.

3. Results and discussion

3.1. *Stress analysis of tubes under effect of superimposed hydrostatic pressure*

3.1.1. *Stress state and yield locus in tube free bulging process*

Theoretically, the external pressure can be as high as the maximum applicable pressure of the pressure boosting device in the double-sided tube hydroforming process. Thus, the stress state of the tube is tri-axial. Fig. 4 shows the simulated stress distribution of the 5A02 aluminum alloy tubes in free bulging under different external pressures when the bulging height reached 3.67 mm. At this instant, the tube was in the last stage of uniform deformation. The circumferential stress, axial stress, and through-thickness normal stress were found to decrease in accordance with an increase in the external pressure. When the external pressure reaches 212.5 MPa, i.e., 2.5 times the yield strength of the 5A02 tube, at the pole of bulging area, its circumferential stress decreases from 230.3 MPa to 17.6 MPa, in addition to its axial stress from 120.9 MPa to −92.1 MPa, and its normal stress from −0.6 MPa to −213.1 MPa. It is a 3D stress state in this case, with the tension in the circumferential direction and compression in the axial and normal directions. Furthermore, the decrease in the three stress components was almost equal to the increase in the external pressure.

Fig. 5 presents the distribution of the hydraulic pressure and Lode parameter of the 5A02 tubes in the free bulging area under different external pressures obtained from the simulation. The hydrostatic pressure on the tube is superimposed with the magnitude of the external pressure, whereas the Lode parameter is not dependent on the imposed external pressure, irrespective of the external pressure level. These simulation results are consistent with the theoretical derivation under the plane strain assumption in the previously published paper [24].

As mentioned above, the circumferential stress, axial stress and through-thickness normal stress all decreased with an increase in the external pressure. However, the occurrence of yielding in double-sided tube hydroforming is directly related to the equivalent stress. Hence, Fig. 6 shows the equivalent stress contour of the 5A02 tubes in the double-sided free bulging with external pressures of 0 MPa and 212.5 MPa. From Fig. 6, it can be seen that the occurrence of yielding under an external pressure of 212.5 MPa is similar to that of the tube hydroforming without external pressure.

The case of the external pressure of 212.5 MPa is used as an example to explain the occurrence of yielding in the double-sided tube free bulging process. From Fig. 6(b), it can be seen that the entire bulging zone of the tube starts to yield when the internal pressure reaches 218.5 MPa. With an increase in the internal pressure, the higher pressure difference drives the tube to bulge, and the deformation is gradually concentrated toward the center of the bulging zone. Thus, an

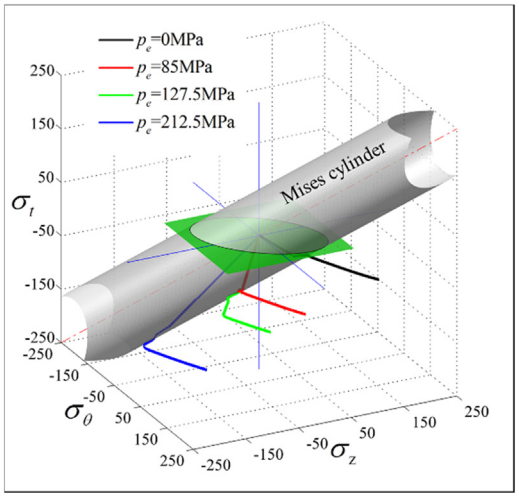

Fig. 7 – Stress locus of 5A02 tube in free bulging under internal and external pressures.

equivalent stress gradient is generated between the center and die entrance, and the maximum equivalent stress is located at the center. When the internal pressure increases to 225 MPa, the equivalent stress gradient is more pronounced. During the bulging process, the maximum bulging height is at the center of the bulging zone, i.e., the pole of the bulging zone.

At the pole of the bulging zone, the maximum equivalent stress is located on the inside surface of the tube. Therefore, the stress components at the point of maximum equivalent stress were determined and described on the von-Mises 3D yield cylinder, to compare the stress loci under different external pressures, as shown in Fig. 7. It can be seen from Fig. 7 that the stress loci can directly visualize the 3D stress states that act on the tube and their development process. Without external pressure (0 MPa), the tube is in a plane stress state, which evolves linearly in the biaxial tensile stress zone of the elliptical yield locus. Once the plane stress state reaches the initial elliptical yield locus, the tube starts to yield. Due to the continuous increase in the internal pressure, the plastic deformation of the tube is maintained, and the stress locus basically develops along the direction of its original trajectory outside the initial yielding ellipse. However, if the external pressure is imposed, the stress path of the tube deviates from the plane stress yielding ellipse at the outset, and it is directed in the negative semi axial direction of the generatrix of the von-Mises yielding cylinder. The stress path evolves linearly until it reaches the von-Mises yielding cylinder, after which the tube materials are deformed. Thereafter, the stress path is re-orientated to the direction parallel to that of the stress trajectory of the 0 MPa external pressure. It can be seen that the stress locus develops in the plane with the normal stress of

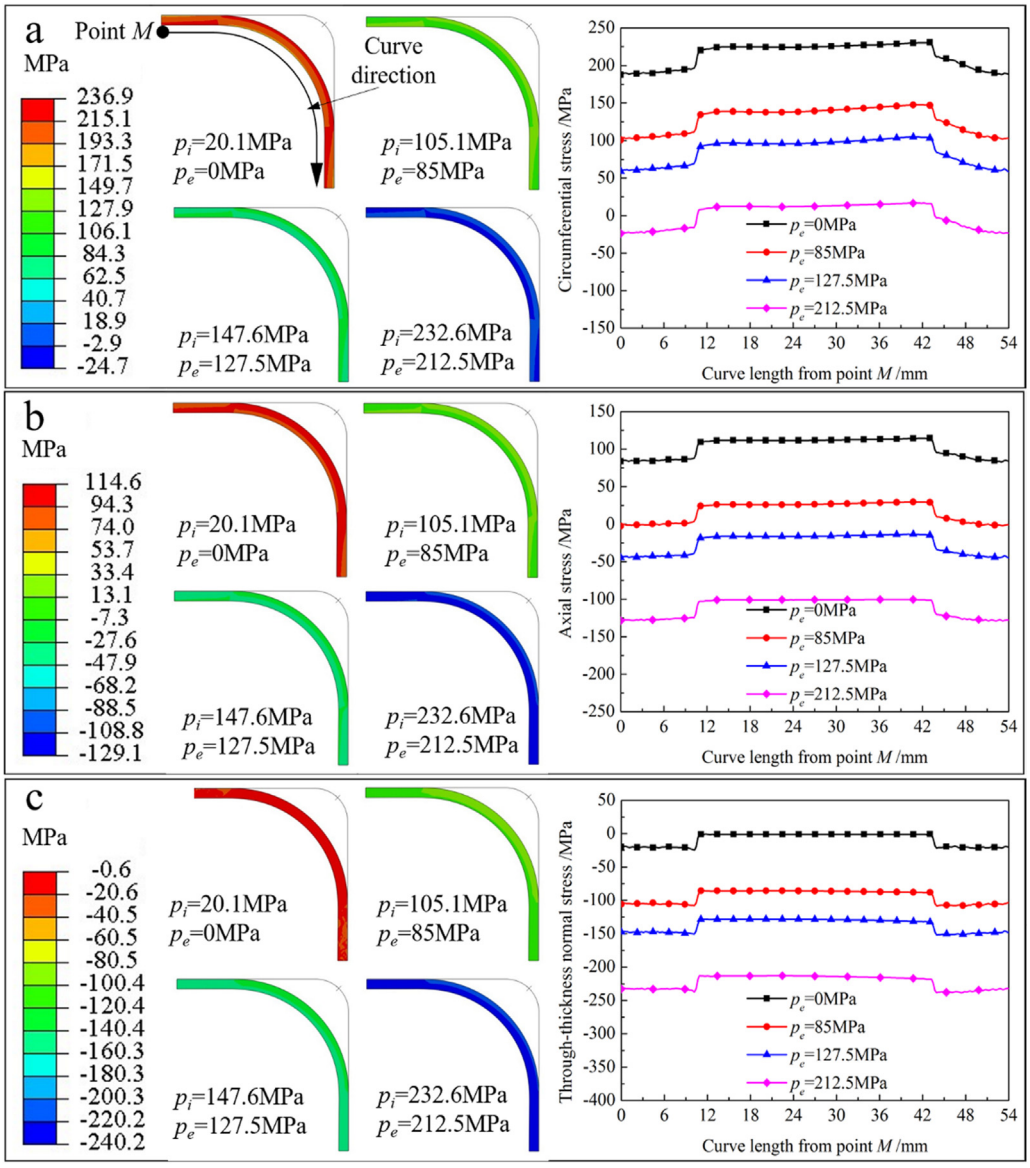

Fig. 8 – Stress distribution of 5A02 tubes in corner filling process under internal and external pressures: (a) circumferential stress; (b) axial stress; (c) normal stress.

$-p_e$ after the tube yields in the double-sided tube free bulging process. In summary, when the tube is bulged under the double-sided pressure with a constant external pressure, the stress locus initiates at the origin co-ordinate and evolves linearly to a plane with a normal stress of $-p_e$. Moreover, the turning point occurs at the stress locus, which leads to its continuous development in the plane with a normal stress of $-p_e$.

3.1.2. *Stress state and yield locus in tube corner filling process*

Fig. 8 shows the stress distribution of the 5A02 tubes in the corner filling process under a pressure difference of 20.1 MPa. From Fig. 8, it can be seen that the variations of all the stress components are similar to those of the abovementioned free bulging process, i.e., a decrease trend in accordance with an increase in the external pressure. Similarly, if the external pressure of 212.5 MPa, which is 2.5 times as big as the yield strength of the 5A02 tube, was imposed on the tube, the circumferential stress would decrease from 224.7 MPa to 12.5 MPa, in addition to the axial stress from 111.6 MPa to −100.7 MPa, and the normal stress from −0.9 MPa to −213.5 MPa. The stress state was clearly translated from an in-plane biaxial tensile stress state to a 3D stress state (tension in the circumferential direction and compression in the axial and normal directions). In addition, the reductions of all three stress components are nearly equal to the increase in the external pressure.

For the hydrostatic pressure and Lode parameter in the tube corner filling process under double-sided pressures, it was also found that the hydrostatic pressure for the tube is

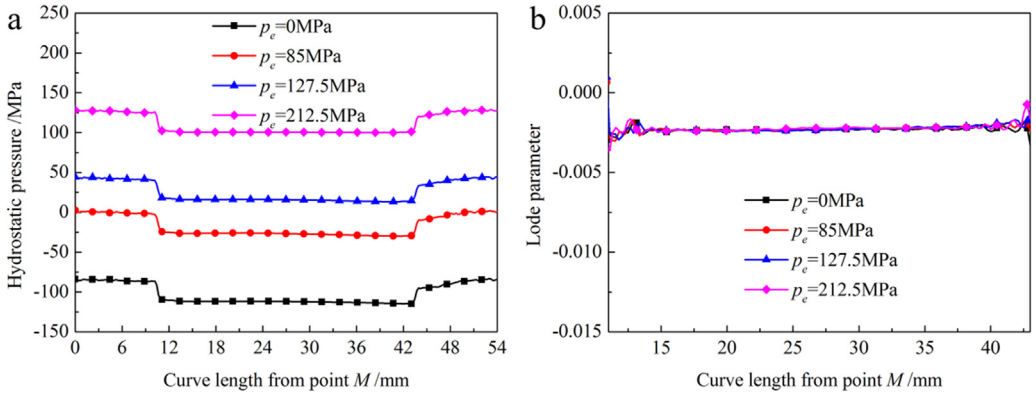

Fig. 9 – Hydraulic pressure and Lode parameter of 5A02 tubes during corner filling process: (a) hydraulic pressure; (b) Lode parameter.

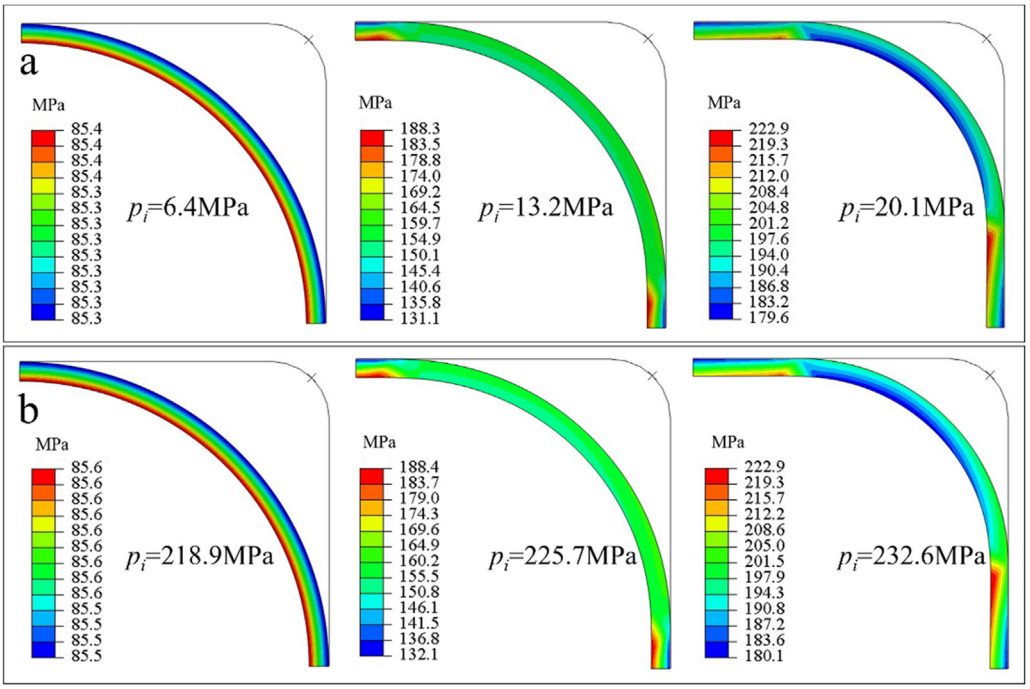

Fig. 10 – Equivalent stress distribution of 5A02 tube during corner filling process under internal and external pressures: (a) p_e = 0 MPa; (b) p_e = 212.5 MPa.

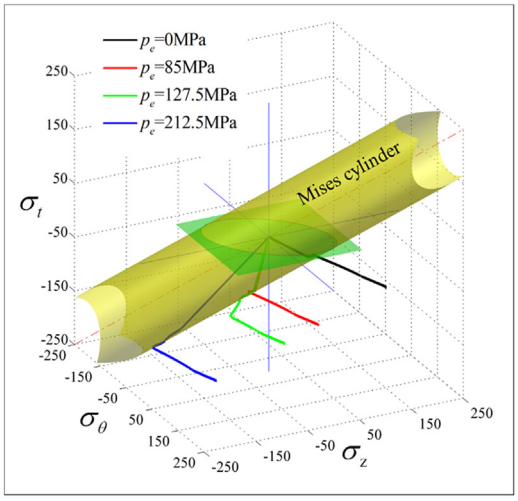

Fig. 11 – Stress locus of 5A02 tube in corner filling process under internal and external pressure.

superimposed with the magnitude of the external pressure, whereas the Lode parameter is not dependent on the imposed external pressure, as shown in Fig. 9. The stress variation with an increase in the external pressure is in good agreement with the results from the double-sided tube free bulging process.

Fig. 10 presents the equivalent stress contour of the 5A02 tubes in the corner filling process with external pressures of 0 MPa and 212.5 MPa. It can be seen from Fig. 10 that the occurrence and development of yielding in the tube corner filling process under double-sided pressures is similar to that of the tube corner filling without external pressure. Moreover, the case of the external pressure of 212.5 MPa is used as an example to explain the occurrence and development of yielding in the tube corner filling process under double-sided pressures.

It can be seen from Fig. 10(b) that there is only a line contact between the tube and square-sectional die cavity before deformation, and the tube yields at the internal pressure of 218.9 MPa. The equivalent stress on the inner surface is greater

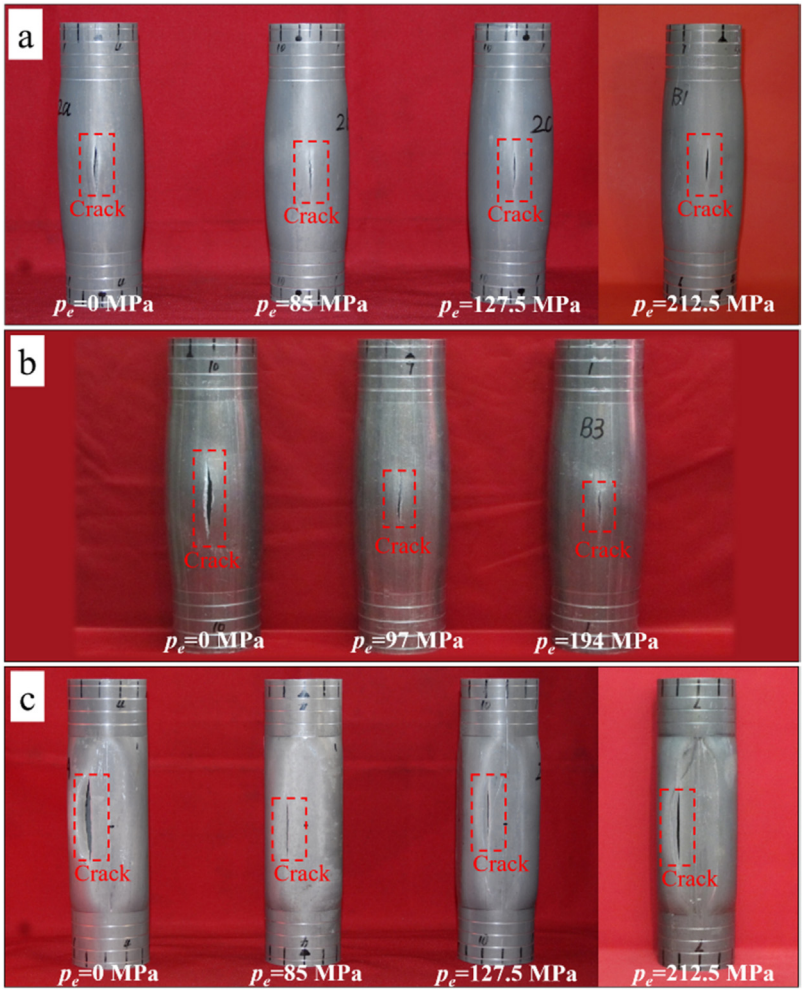

Fig. 12 – Cracked aluminum alloy tubes obtained via double-sided hydroforming process: (a) free bulging of 5A02 aluminum alloy tubes (image partially obtained from Ref. [24]); (b) free bulging of 2A12 aluminum alloy tubes; (c) corner filling of 5A02 aluminum alloy tubes (image partially obtained from Ref. [24]).

than that on the outer surface, which result in a stress gradient along the direction of thickness. As the internal pressure increases, the tube bulges toward to the die corner and attaches to the straight wall of the die cavity. When the internal pressure increases to 225.7 MPa, the maximum equivalent stress is located on the inner surface of the attached area. As the corner filling process progress, the contact area between the tube and die cavity gradually increases, and the filet radius of the tube decrease. During this process, the maximum equivalent stress is always located on the inner surface of the transition region, which led to the maximum deformation and the final fracture.

The stress locus at a point on the inner surface of the transition region was described on the von-Mises 3D yield cylinder for different external pressure conditions, as shown in Fig. 11. From Fig. 11, it can be seen that the stress locus on the von-Mises yield cylinder for the double-sided tube corner filling process is the same as that for the double-sided tube free bulging process (see Fig. 7).

3.2. *Fracture behavior of tubes under effect of superimposed hydrostatic pressure*

3.2.1. *Cracked aluminum alloy tubes*

Fig. 12 shows three types of cracked aluminum alloy tubes from the double-sided hydroforming process, the cracked 5A02 aluminum alloy and cracked 2A12 aluminum alloy tubes from the double-sided free bulging, and the cracked 5A02 aluminum alloy tubes from the double-sided tube corner filling process. For the consistency of the initial tubes, a longer tube was divided into several tube samples for the same experiment, to eliminate the interference of the performance difference and the difference in the initial thickness. From Fig. 12(a) and (b), it can be seen that the fracture occurred at the pole of the bulging area. Moreover, from Fig. 12(c), it can be seen that the fracture favored the transition region. This is due to greater stresses at these regions, as discussed in Section 3.1. It was also found that the fracture develops along the axial direction under double-sided pressures. This is different from the case in Ref. [25], in which the fracture developed in the circumferential direction.

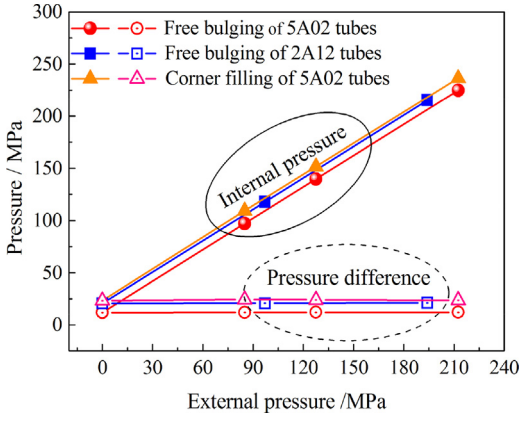

Fig. 13 – Fracture pressures for tube in free bulging and corner filling under internal and external pressures.

The internal pressure and pressure difference at the fracture moment are presented in Fig. 13. It should be noted that, as shown in Fig. 13, the pressure difference at the fracture moment is insensitive to the external pressure in both the double-sided tube free bulging process and double-sided tube corner filling process.

3.2.2. *Fracture morphology*

Fig. 14 shows the effect of the external pressure, i.e., the superimposed hydrostatic pressure, on the fracture morphology of the 5A02 aluminum alloy and 2A12 aluminum alloy tubes in the double-sided free bulging and corner filling experiments. From a comparison of the fracture morphologies of the tubes, as can be seen in Fig. 14, numerous equiaxial dimples with significant depths were present on the fractured surface of the tube without any external pressure applied to its outer surface. Upon the application of the external pressure, the higher hydrostatic pressure decreased the depth of the equiaxial dimples on the fractured surface, and their number, size, and proportion all decreased with an increase in the external pressure. Moreover, as the external pressure increased, the direction of the dimples changed. For example, the direction of the dimples is the same as that of the circumferential tensile stress when the external pressure is 0; however, an increase in the external pressure could alter the direction of the dimples, and divert it to another direction, which may result in drag marks on the fractured surface. This is because the fracture mode of the tube shifts from the micro void accumulation fracture to shear fracture with an increase in the external pressure. Especially for the 5A02 aluminum alloy tubes in double-sided corner filling process, only a few dimples were presented on the fractured surface when the external pressure reached 212.5 MPa ($2.5\sigma_s$). Hence, it is approximately dominated by the pure shear fracture.

Based on the discussion above, it was concluded that the higher external pressure can not only change the type, number, size, and proportion of the dimples on the fractured surface, but also transform the fracture mode from a void accumulation fracture to a pure shear fracture. The results are similar to those in the published paper [25], which stated that the fracture surface of sheets and hydroformed tubes shifted from a planar (P-type) profile to a chisel (C-type) shape in accordance with an increase in the superimposed hydrostatic pressure increases.

3.2.3. *Fracture strain*

Fig. 15 presents the SEM images with a 100× magnification of the fracture surface, for the estimation of the thickness of the tubes at fracture, *t*. In Fig. 15, the subscript of *t* denotes the ratio of the external pressure to the yield strength of the tube.

After the measurement of the thickness at the fracture, it was found that $t_{0.0} = 0.78$ mm, $t_{1.0} = 0.60$ mm, $t_{1.5} = 0.42$ mm, and $t_{2.5} = 0.22$ mm for the double-sided free bulging of the 5A02 aluminum alloy tubes; $t_{0.0} = 2.37$ mm, $t_{1.0} = 1.96$ mm, and $t_{2.0} = 1.26$ mm for the double-sided free bulging of 2A12 aluminum alloy tubes; and $t_{0.0} = 0.94$ mm, $t_{1.0} = 0.66$ mm, $t_{1.5} = 0.46$ mm, and $t_{2.5} = 0.14$ mm for the double-sided corner filling of 5A02 aluminum alloy tubes. Thus, it was concluded from the measurement results that an increase in the external pressure results in a decrease in the thickness at fracture in the

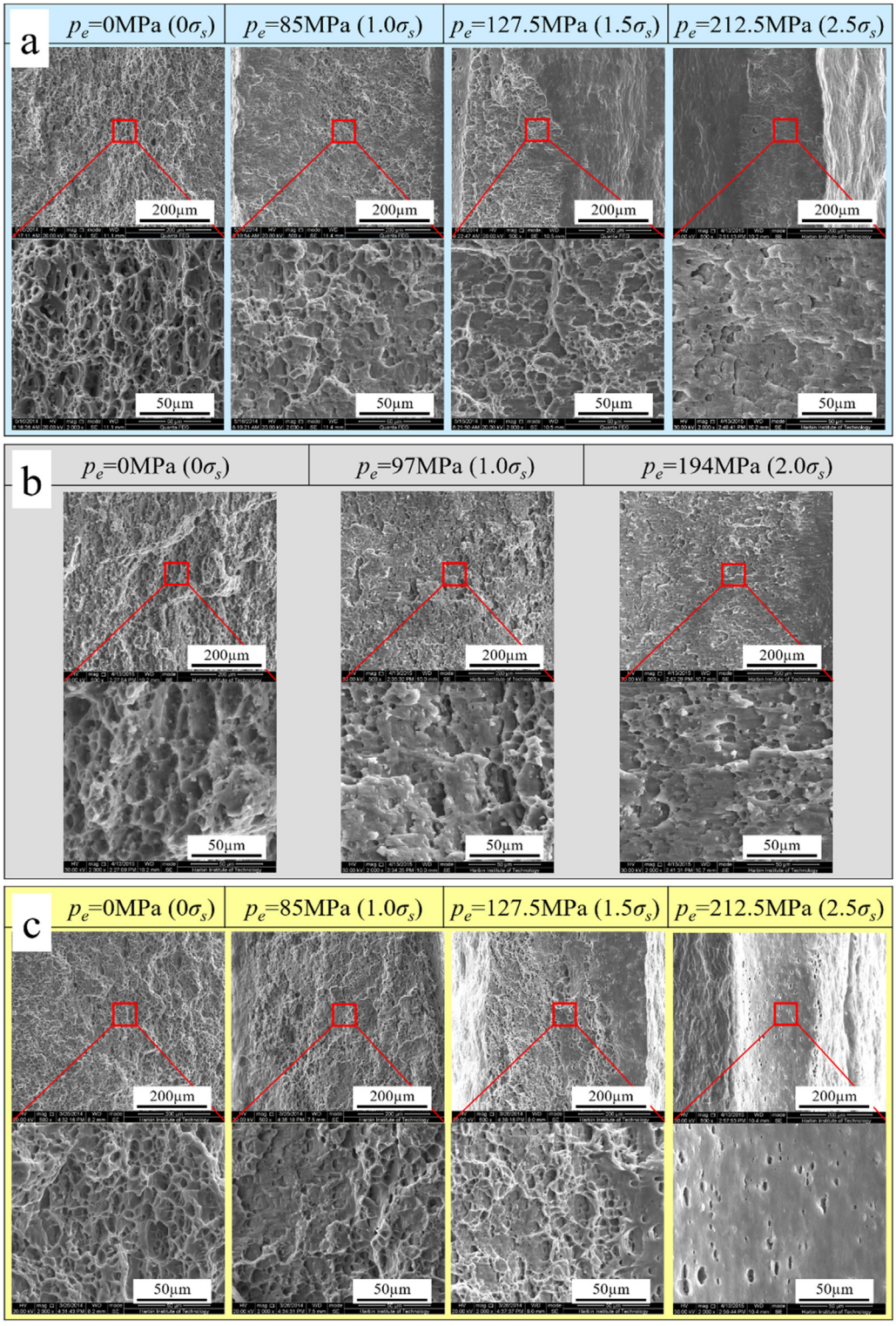

Fig. 14 – Effect of external pressure on fracture morphology of tubes under internal and external pressures: (a) free bulging of 5A02 tubes; (b) free bulging of 2A12 tubes; (c) corner filling of 5A02 tubes (image partially obtained from Ref. [24]).

double-sided tube free bulging process and double-sided tube corner filling process, or the different tubes that were used.

Fig. 16 presents the thickness strain at fracture of the different tubes under different external pressures. It can be seen from Fig. 16 that the thickness compressive strain at the fracture increased gradually with an increase in the external pressure, and the amplitude increases simultaneously.

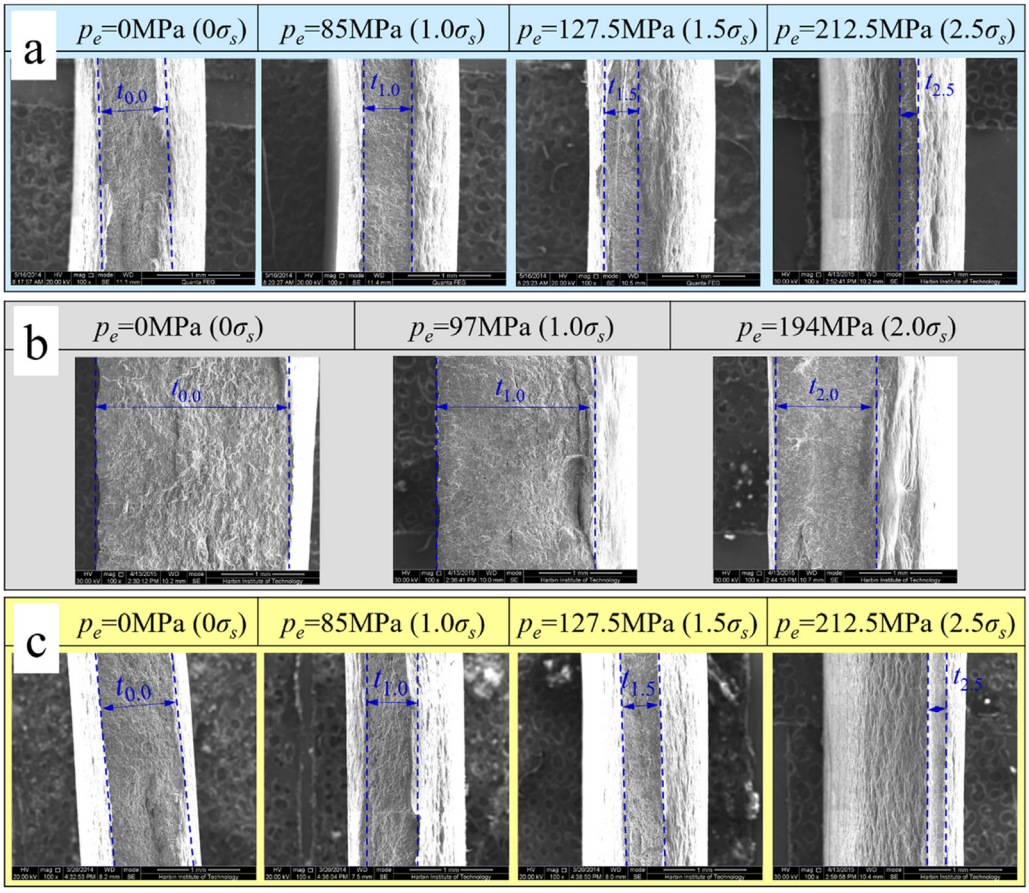

Fig. 15 – Effect of external pressure on thickness of tubes at fracture under internal and external pressures: (a) free bulging of 5A02 tubes; (b) free bulging of 2A12 tubes; (c) corner filling of 5A02 tubes (image partially obtained from Ref. [24]).

Assuming that the tube has a plane strain fracture in the longitudinal direction, i.e., the axial strain $\varepsilon_z = 0$, the relationship between the circumferential stain ε_θ and through-thickness normal strain ε_t is $\varepsilon_\theta = -\varepsilon_t$ based on the incompressibility of the tube. Therefore, the equivalent fracture strain of the tubes can be expressed as follows:

$$\epsilon_f = \frac{2}{3}\sqrt{\epsilon_\theta^2 - \epsilon_\theta\epsilon_t + \epsilon_t^2} = \frac{2}{\sqrt{3}}|\epsilon_t| \tag{1}$$

From Eq. (1), it can be seen that the equivalent fracture strain of the tubes can be directly calculated from the thickness strain at fracture. Thus, by substituting the thickness strain at fracture, as shown in Fig. 16, into Eq. (1), the equivalent fracture strain of the tubes under different external pressures can be calculated, as shown in Fig. 17. It can be found from Fig. 17 that the equivalent fracture limits of the tubes can be significantly improved by increasing the external pressure. For the 5A02 aluminum alloy tubes, when the external pressure increased from 0 MPa to 212.5 MPa (2.5σ_s), the equivalent fracture strain increased from 1.022 to 2.466 in the free bulging process, which corresponds to an increase of 141.3%. Moreover, the equivalent fracture strain increased from 0.860 to 3.054 in the corner filling process, which corresponds to an increase of 255.1%. Furthermore, the influence of the external pressure on the 2A12 aluminum alloy tubes in the free bulging process is similar to that of the 5A02 tubes, and its equivalent fracture strain increased from 0.227 to 0.956, which corresponds to an increase in amplitude of 321.1%.

With respect to the mechanism of the external pressure effect on the fracture limit, it is attributed to the increased superimposed hydrostatic pressure due to the imposed external pressure, which can strongly inhibit the nucleation, growth, and coalescence of micro voids, thus increasing the fracture strain of the tubes [10].

4. Conclusions

In this investigation, the finite element analysis and experiments were conducted to investigate the bulging deformation and fracture of tubes in double-sided hydroforming. The effect of the superimposed hydrostatic pressure, which is determined by the external pressure, on the stress state, yield

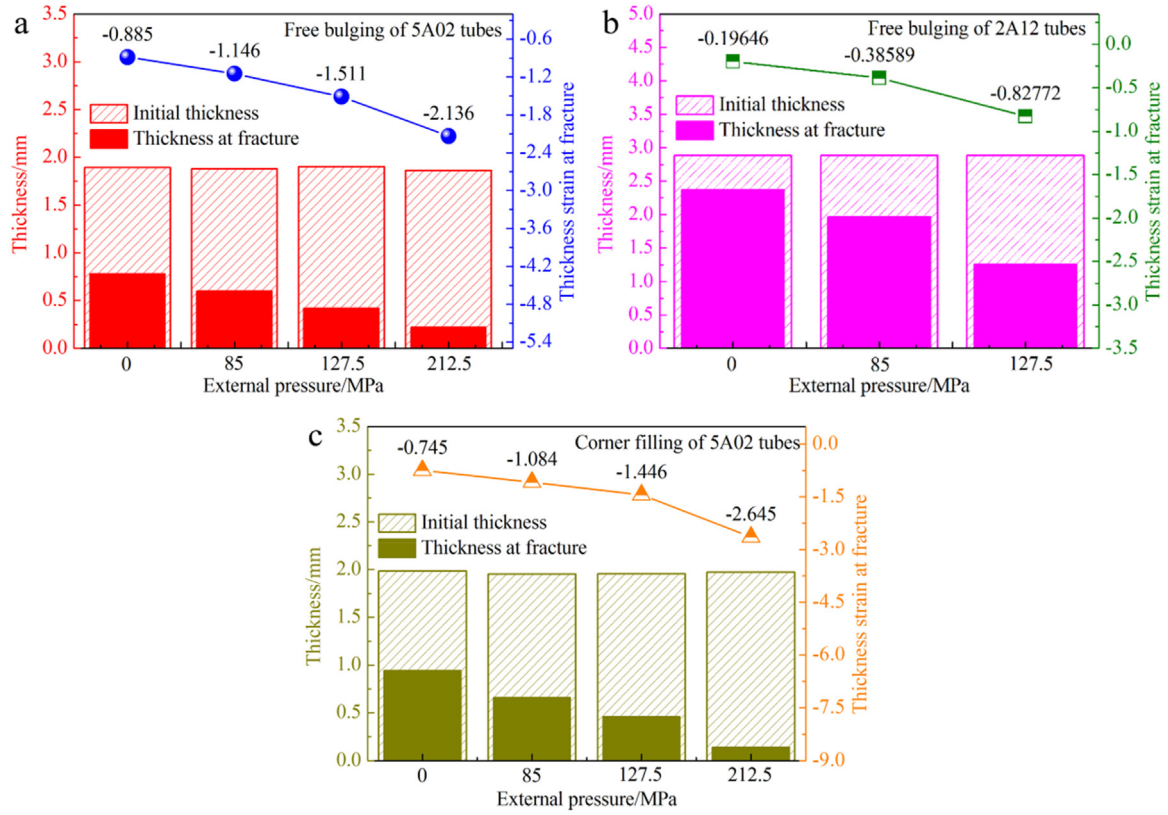

Fig. 16 – Effect of external pressure on the thickness strain at fracture of tubes: (a) free bulging of 5A02 tubes; (b) free bulging of 2A12 tubes; (c) corner filling of 5A02 tubes (image partially obtained from Ref. [24]).

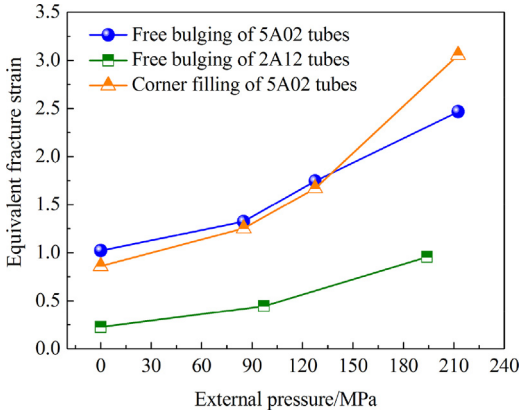

Fig. 17 – Effect of external pressure on the equivalent fracture strain of tubes under double-sided pressures.

development, fracture surface formation, and fracture limit strain of the tubes was evaluated. The following conclusions can be drawn from the above discussion:

(1) The external pressure has a significant impact on the stress state of the tube in the double-sided hydroforming process. Under a sufficiently high external pressure, the stress state can change from an in-plane biaxial tensile stress state to a three-dimensional stress state (tension in the circumferential direction and compression in the axial and normal directions), and the reductions of all the three stress components are nearly equal to the increase in external pressure. Moreover, the hydrostatic pressure for the tube was superimposed with the magnitude of the external pressure, whereas the Lode parameter is not dependent on the imposed external pressure.

(2) When the tubes are hydroformed under the double-sided pressure with a constant external pressure in the double-sided free bulging or corner filling processes, their stress loci initiate at the coordinate origin and evolve linearly to a plane with a normal stress of $-p_e$. The turning points then occur at the stress loci, which lead to their continuous development in the plane with a normal stress of $-p_e$.

(3) The experimental results for the 5A02 aluminum alloy and 2A12 aluminum alloy tubes revealed that the fracture of the tubes develops along their axial direction under double-sided pressures. Moreover, it was concluded that the higher external pressure could change the type, number, size, and proportion of the dimples on the fractured surface of the tubes, and transform the fracture mode from a void accumulation fracture to a pure shear fracture.

(4) The fracture limits of the tubes can be significantly improved by increasing the external pressure. This is mainly because the superimposed hydrostatic pressure, which is determined by the external pressure, can strongly

inhibit the nucleation, growth, and coalescence of micro voids. For the 5A02 aluminum alloy tubes, their equivalent fracture strains increased by 141.3% and 255.1% in the double-sided free bulging and corner filling, respectively, when the external pressure reached $2.5\sigma_s$. For the 2A12 aluminum alloy tubes, the increase in the amplitude of the equivalent fracture strain reached 321.1% when the external pressure was 194 MPa ($2.0\sigma_s$).

It should be noted that this work is significant for the consolidation of the theoretical and numerical simulation prediction of the superimposed hydrostatic pressure effect in the tube hydroforming process. In addition, it also can be used to support the development of a ductile fracture criterion considering the stress triaxiality and the Lode parameter.

Ethical statement

Authors state that the research was conducted according to ethical standards.

Funding

This study presented herein is financially supported by National Natural Science Foundation of China (Grant No: 51805357, U1637209).

Acknowledgments

This study presented herein is financially supported by National Natural Science Foundation of China (Grant No: 51805357, U1637209). The authors wish to express their gratitude to the funding.

REFERENCES

[1] R. Bihamta, Q.-H. Bui, M. Guillot, G. D'Amours, A. Rahem, M. Fafard, Global optimisation of the production of complex aluminium tubes by the hydroforming process, CIRP J. Manuf. Sci. Technol. 9 (2015) 1–11. http://dx.doi.org/10.1016/j.cirpj.2015.02.001.

[2] H.Y. Li, X.S. Wang, S.J. Yuan, Q.B. Miao, Z.R. Wang, Typical stress states of tube hydroforming and their distribution on the yield ellipse, J. Mater. Process. Technol. 151 (2004) 345–349. http://dx.doi.org/10.1016/j.jmatprotec.2004.04.085.

[3] E. Chu, Y. Xu, Hydroforming of aluminum extrusion tubes for automotive applications. Part I: buckling, wrinkling and bursting analyses of aluminum tubes, Int. J. Mech. Sci. 46 (2004) 263–283. http://dx.doi.org/10.1016/j.ijmecsci.2004.02.014.

[4] Y.P. Korkolis, S. Kyriakides, Inflation and burst of anisotropic aluminum tubes for hydroforming applications, Int. J. Plast. 24 (2008) 509–543. http://dx.doi.org/10.1016/j.ijplas.2007.07.010.

[5] M. Liewald, R. Pop, Magnesium tube hydroforming, Materwiss. Werksttech. 39 (2008) 343–348. http://dx.doi.org/10.1002/mawe.200800303.

[6] A.A. Luo, A.K. Sachdev, 11 – Bending and hydroforming of aluminum and magnesium alloy tubes, in: M. Koç (Ed.), Hydroforming Adv. Manuf., Woodhead Publishing, 2008 238–266. http://dx.doi.org/10.1533/9781845694418.2.238.

[7] X. Guo, F. Ma, Q. Guo, X. Luo, N. Kim, K. Jin, A calculating method of tube constants of ductile fracture criteria in tube free bulging process based on M-K theory, Int. J. Mech. Sci. (2017), http://dx.doi.org/10.1016/j.ijmecsci.2017.04.012.

[8] Y. Lou, H. Huh, Extension of a shear-controlled ductile fracture model considering the stress triaxiality and the Lode parameter, Int. J. Solids Struct. 50 (2013) 447–455. http://dx.doi.org/10.1016/j.ijsolstr.2012.10.007.

[9] P.W. Bridgman, Studies in Large Plastic Flow and Fracture, With Special Emphasis on the Effects of Hydrostatic Pressure, McGraw-Hill, New York, 1952, http://dx.doi.org/10.4159/harvard.9780674731349.

[10] J.J. Lewandowski, P. Lowhaphandu, Effects of hydrostatic pressure on mechanical behaviour and deformation processing of materials, Int. Mater. Rev. 43 (1998) 145–187. http://dx.doi.org/10.1179/imr.1998.43.4.145.

[11] J.A. Sauer, D.R. Mears, K.D. Pae, Effects of hydrostatic pressure on the mechanical behaviour of polytetrafluoroethylene and polycarbonate, Eur. Polym. J. 6 (1970) 1015–1032. http://dx.doi.org/10.1016/0014-3057(70)90034-0.

[12] I.E. French, P.F. Weinrich, C.W. Weaver, Tensile fracture of free machining brass as a function of hydrostatic pressure, Acta Metall. 21 (1973) 1045–1049. http://dx.doi.org/10.1016/0001-6160(73)90020-5.

[13] I.E. French, P.F. Weinrich, The influence of hydrostatic pressure on the tensile deformation and fracture of copper, Metall. Trans. A 6 (1975) 785, http://dx.doi.org/10.1007/BF02672300.

[14] A. Brownrigg, W.A. Spitzig, O. Richmond, D. Teirlinck, J.D. Embury, The influence of hydrostatic pressure on the flow stress and ductility of a spherodized 1045 steel, Acta Metall. 31 (1983) 1141–1150. http://dx.doi.org/10.1016/0001-6160(83)90176-1.

[15] D.S. Liu, J.J. Lewandowski, The effects of superimposed hydrostatic pressure on deformation and fracture: Part I. Monolithic 6061 aluminum, Metall. Trans. A 24 (1993) 601–608. http://dx.doi.org/10.1007/BF02656629.

[16] J. Peng, P.D. Wu, Y. Huang, X.X. Chen, D.J. Lloyd, J.D. Embury, K.W. Neale, Effects of superimposed hydrostatic pressure on fracture in round bars under tension, Int. J. Solids Struct. 46 (2009) 3741–3749. http://dx.doi.org/10.1016/j.ijsolstr.2009.07.001.

[17] P.D. Wu, X.X. Chen, D.J. Lloyd, J.D. Embury, Effects of superimposed hydrostatic pressure on fracture in sheet metals under tension, Int. J. Mech. Sci. 52 (2010) 236–244. http://dx.doi.org/10.1016/j.ijmecsci.2009.09.14.

[18] F.J. Fuchs, Hydrostatic pressure: its role in metal forming, Mech. Eng. (1966) 34–40.

[19] L.M. Smith, S. Ganeshmurthy, K. Alladi, Double-sided high-pressure tubular hydroforming, J. Mater. Process. Technol. 142 (2003) 599–608. http://dx.doi.org/10.1016/S0924-0136(02)01041-5.

[20] F. Zhang, J. Chen, J. Chen, X. Zhu, Forming limit model evaluation for anisotropic sheet metals under through-thickness normal stress, Int. J. Mech. Sci. 89 (2014) 40–46. http://dx.doi.org/10.1016/j.ijmecsci.2014.08.016.

[21] J.M. Allwood, D.R. Shouler, Generalised forming limit diagrams showing increased forming limits with non-planar stress states, Int. J. Plast. 25 (2009) 1207–1230. http://dx.doi.org/10.1016/j.ijplas.2008.11.001.

[22] X.-L. Cui, X.-S. Wang, S.-J. Yuan, Deformation analysis of double-sided tube hydroforming in square-section die, J.

Mater. Process. Technol. 214 (2014), http://dx.doi.org/10.1016/j.jmatprotec.2014.02.005.

[23] X.-L. Cui, X.-S. Wang, S.-J. Yuan, The bulging behavior of thick-walled 6063 aluminum alloy tubes under double-sided pressures, JOM 67 (2015), http://dx.doi.org/10.1007/s11837-015-1291-1.

[24] X.L. Cui, X.S. Wang, S.J. Yuan, Experimental verification of the influence of normal stress on the formability of thin-walled 5A02 aluminum alloy tubes, Int. J. Mech. Sci. 88 (2014) 232–243. http://dx.doi.org/10.1016/j.ijmecsci.2014.07.011.

[25] Y. Shi, H. Jin, P.D. Wu, D.J. Lloyd, Effects of superimposed hydrostatic pressure on necking and fracture of tube under hydroforming, Int. J. Solids Struct. (2017), http://dx.doi.org/10.1016/j.ijsolstr.2017.02.027.